 doi:10.20944/preprints201805.0171.v1

Article

Fracture Reconstruction and Analysis of Low Permeability Carbonates using x-ray Tomography for Comparison with Outcrop Data

Stephanie G Zihms [1]*, Helen Lewis [1], Tiago Siqueira de Miranda [2], Stephen Hall [3] and James Somerville[1]

[1] Institute of Petroleum Engineering, Heriot-Watt University, Edinburg, UK
[2] Department de Geologia, Universidade de Tecnologia de Pernambuco, Recife, Brazil
[3] Division of Solid Mechanics, Lund University, Lund, Sweden
* Correspondence: s.zihms@hw.ac.uk; Tel.: +44-(0)-131-3845

Abstract: Comparing outcrop data to laboratory results is important to verify and validate experiments of analogue and reservoir materials especially regarding conditions for deformation experiments. This is important better understand highly complex carbonate reservoir strata and their response to changes in subsurface conditions, reducing subsurface uncertainty. This study develops methods to allow for a more straightforward comparison of outcrop data (m-scale) with experimentally created fracture arrays developed in cylindrical samples (cm-scale). The main objective is to assess usefulness of experimentally-produced fracture networks as analogues for subsurface structures, typically at the meter and above scale by developing new techniques to use the lab deformation. It analyses key characteristics of laboratory-induced fracture networks by adapting scanline methods to use with x-ray tomography (XRT) images to allow for comparison with outcrop and field data. To test and verify these new methods two low permeability carbonate samples were used for deformation testing and analysis. Applying the different scanline methods we show that they can be used to analyse lab induced fractures (mm to cm-scale) identified in XRT images for comparison with outcrop data (m-scale). In addition, these methods also allow for quantification of fracture network attributes e.g. fracture spacing, fracture apertures, orientation. This new data bridges the gap between micro-scanlines using thin sections and outcrop scanlines.

Keywords: fractures, geomechanics, carbonates, multi-scale, x-ray tomography

1. Introduction

To allow for a better comparison between laboratory (mm to cm-scale) and field (m-scale) data sets we present two techniques that both utilise x-ray tomography (XRT) images. By quantifying certain aspects of the fracture network (e.g. intersection with XRT image edge or fracture aperture) these methods allow for detailed analysis and reconstruction of fracture networks that can be used to compare with outcrop data directly. Comparing outcrop data to laboratory results is important to verify and validate experiments of analogue and reservoir materials especially regarding conditions for deformation experiments, especially since experimental results help to populate geomodels with subsurface structural features, particularly where data is sparse. Important properties are fracture distribution and fracture connectivity, since they have the potential to provide major pathways for fluids in the subsurface, especially in low porosity carbonates, as well as other low porosity rocks [1-4].

XRT is becoming a widely used non-destructive technique in geoscience to assess and characterise rocks. It has been used successfully on a range of different rock types, as well as non-geological materials [5-12]. Imaging limitations are related to sample size and its relation to image resolution. With more powerful XRT acquisitions imaging standard 38mm diameter 76mm length

 doi:10.20944/preprints201805.0171.v1

core plugs is possible. However, XRT studies on carbonates tend to focus on characterisation of pore networks, rock characterisation or permeability calculations to aid characterisation relevant for petroleum engineering purposes such as prediction of permeability, or pore network connectivity [5, 9, 11, 13-15]. A few studies use XRT to identify fractures or similar features within the core samples [16]. But the majority of studies appear to be limited to non-destructive characterisation of rock properties (e.g. porosity, grain shape, grain size) to allow for a faster characterisation. This study aims to analyse key characteristics of laboratory-induced fracture networks to allow for comparison with outcrop and field data.

Laminites from the Crato Formation (NE Brazil) are a suitable analogue for the Brazilian pre-salt oil-bearing carbonate reservoir rocks (Miranda et al., 2014, Santos et al., 2015, Catto et al., 2016). Considering the high risks associated with producing these very deep and highly complex carbonate reservoir rock systems, and the relatively small amount of information about these subsalt reservoir rocks, it is important to better quantify what controls their structural evolution, the fracture, deformation band and fault systems that develop and the resulting response of these rocks to the evolving subsurface conditions

Some carbonates follow the same general pattern of response to that of clastic rocks in terms of response to stress or pressure changes e.g. Oolitic limestones [17-20]. However laminites are finely layered carbonates and cannot be linked to clastic behaviour as easily. Available deformation behaviour or mechanical response observations appear to be limited to field observations [21]. This work describes outcrop logging of loop bedding orientations and SEM analysis methods related to field observations of structural discontinuities, their geometry and distribution across a range of sizes.

2. Materials and Methods

2.1. Sample preparation

The laminite sample (provided by Universidade Federal do Rio de Janeiro (UFRJ)) was 22.41cm long, 10.35cm wide and 5.92cm high (Figure 1), is of Aptian age and was collected from the Mina Triunfo quarry in the Araripe Basin, NE Brazil. The geological history of the Araripe Basin and its laminites is beyond the scope of this paper but they are regarded as suitable analogues for pre-Salt laminites that are now offshore Brazil (Ponte & Appi, 1990; Ponte & Ponte Filho, 1996; Neumann, 1999; Assine, 2007; Miranda, 2014; Miranda, 2016).

Due to the vulnerability of laminae to breaking off during coring only three 38mm diameter core samples perpendicular to laminations were produced to test these new methods. The lamination is mostly mm-scale with a several mm thick band of higher porosity material as shown in figure 1b. Three samples were prepared but the experimental deformation of the 3rd sample was terminated when the sample developed a flaw. Table 1 summarises sample dimension.

Preprints (www.preprints.org) | NOT PEER-REVIEWED | Posted: 10 May 2018 doi:10.20944/preprints201805.0171.v1

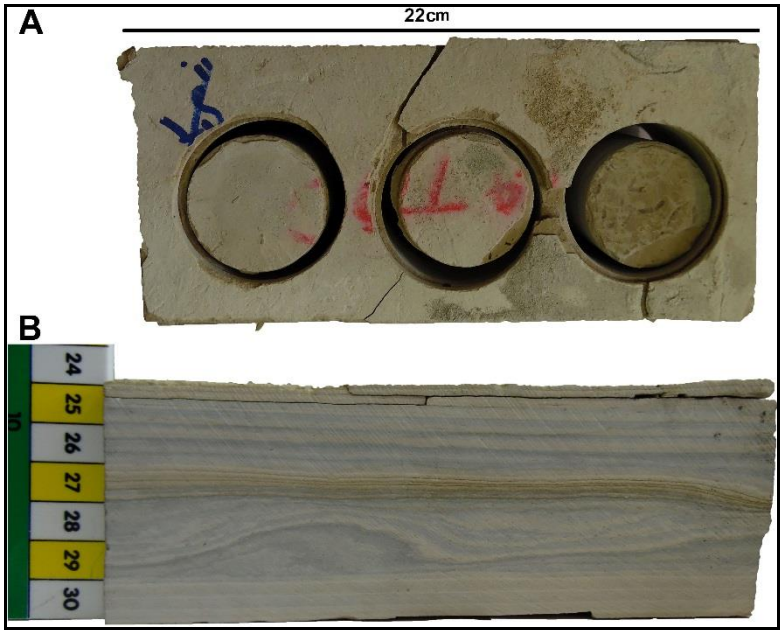

Figure 1. Laminite outcrop sample from Mina Triunfo quarry, NE Brazil A: top view of the sample showing the plug locations B: side view showing the laminations. More porous portion at about 27 on the scale.

Table 1. Laminite core plug information.

Sample ID	Length	Diameter
	average	
	mm	mm
L-20	53.19	37.77
L-30	51.88	37.74

2.2 Triaxial deformation

Triaxial deformation is used to place the samples under an approximation to the subsurface stress state of interest, where axial force is provided by pistons approaching each other and the lateral load is provided by pressurised fluids. Even though this approach is only an approximation to the true loading path during burial and structural development, this type of experiment regarded as a key factor in understanding and predicting the deformation response via a knowledge base for a set of known conditions. Here only two suitable samples were available. The deformation features developed in the samples are the focus of the remainder of this study

The samples were placed in a Hoek cell and deformed under triaxial conditions with confining pressures of 20 for sample L-20 and 30MPa for sample L-30. Both samples were deformed with a constant shortening rate of 0.55 mm/min. Once peak stress was reached and the axial force started to decrease, a very good indicator that the sample was being damaged, and the test was stopped as quickly as possible. This was done to minimise overwriting of early deformation features by later features. After the test was stopped the sample was carefully extracted from the Hoek cell and photographed. The stress-strain relationship curves for the triaxial deformations are shown below in Figure 5.

 doi:10.20944/preprints201805.0171.v1

2.3 X-ray tomography

XRT was performed at the 4D-Imaging Lab at the Division of Solid Mechanics, Lund University, using a Zeiss XRadia XRM520 X-ray tomograph. For these images, the X-ray tube voltage and power was set to 150 kV and 10 W and the He3 filter was utilised to avoid beam hardening artefacts. The samples were placed at 35, 70 and 80 mm from the source and at 47, 54 and 232 mm. 1601 radiographs were acquired over 360 with an exposure time of 2 or 10 s per projection. The tomographic reconstruction provided a cylindrical image of a vertical section of the sample with both diameter and height of about 1000 voxels, where the voxel is cubic with side lengths of 40 or 10 microns. The tomographic reconstruction was performed using the Zeiss reconstructor software with a correction for the centre of rotation. Sample L-30 was imaged three times exploring different settings whereas sample L-20 was only imaged once.

2.4 Surface fracture reconstruction from XRT – Edge scanline method

Scanlines are a sampling method used to gather fracture traces characteristics e.g. number, length, orientation, aperture [22, 23]. To make this field method suitable for use with XRT images we amended the circular scanline [22, 23] to the edge scanline method. This allows us to record the angle of intersections between fractures and the XRT image edge. Figure 3 shows an example of this technique. For each laminite plug every hundredth image was uploaded into FIJI [24] to collect data using the edge scanline method. Afterwards all recorded edge intersection angles were plotted against core plug depth to produce a 2D fracture surface reconstruction for each sample.

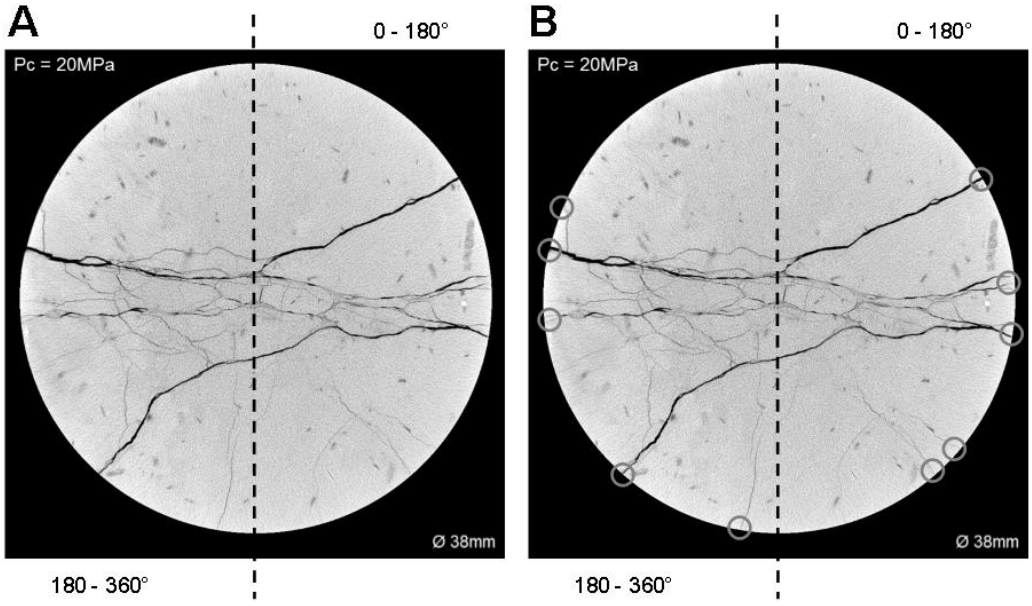

Figure 3. XRT edge scanline technique using individual XRT images. A: division of XRT image into two sections: 0-180° and 180 -360°. B: Example of fracture intersections for angle measurements

2.5 Fracture aperture distribution

For each sample, the middle section of the reconstructed XRT images was isolated (see yellow box in Figure 4) to restrict the scanline area for measurements of fracture aperture and fracture spacing. This technique follows the P10 method [25] which excludes overall lengths of fractures and minimises bias due to sample size. This approach was chosen to eliminate the impact of the core size limiting maximum fracture length to 38mm. To increase contrast between fractures and rock the images were coloured using the Fire overlay available within FIJI. Scanline values for every hundredth slice were taken using scaled XRT images in combination with the built in measuring tool in FIJI. Figure 4 shows an example of this technique.

Preprints (www.preprints.org) | NOT PEER-REVIEWED | Posted: 10 May 2018 doi:10.20944/preprints201805.0171.v1

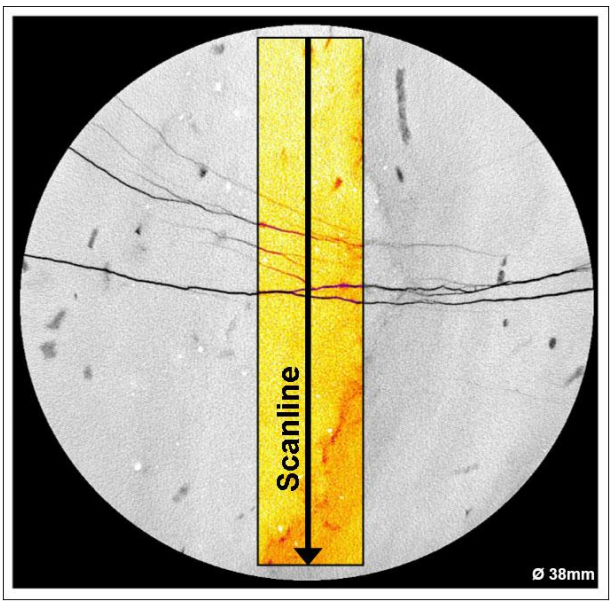

Figure 4. Scanline selection and orientation for fracture aperture measurements from XRT images for lab-induced laminite fractures

3. Results & Discussion

These new techniques allow for comparison of experimental data of laboratory-induced fracture networks with outcrop derived fracture data across several length scales without correction for scale differences between data sets. The ability to make this type of comparison is important to validate experimental procedure and conditions, verify the suitability of core samples for fracture network analysis and help identify any correlation between experimental and outcrop data. The methods shown here make such a comparison tractable. Since similar XRT data from experiments is used in digital rock analysis e.g. for permeability and porosity analysis [14, 26, 27] or to predict fracture fluid-flow [26, 28] it is important to compare experimental and field data to understand how representative the experimental data are.

3.1 Triaxial deformation

Photographs taken of the core plugs after triaxial deformation and removal from the Hoek cell show similar response to loading compared to outcrop observations of structural features [29, 30]. Both samples L20 and L30 show a combination of shear and now-open (at atmospheric pressure) fractures after deformation (Figure 6). Now-open fractures do not show any apparent offset and it is not clear if these are open under confining pressure, and by implication that any natural equivalents are open in the subsurface. It is very likely that these fractures opened during the unloading following triaxial deformation.

Preprints (www.preprints.org) | NOT PEER-REVIEWED | Posted: 10 May 2018 doi:10.20944/preprints201805.0171.v1

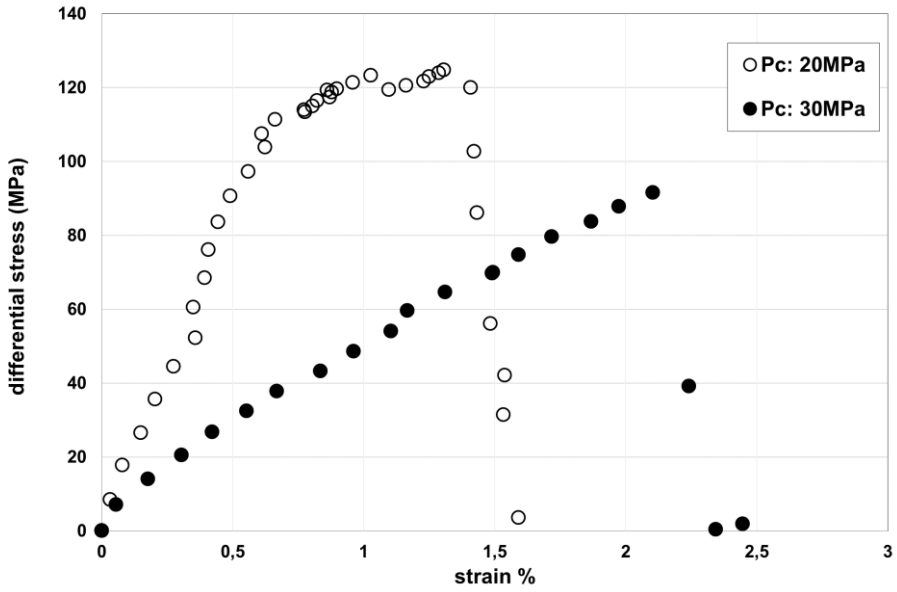

Figure 5. Stress-strain curves for the laminites during triaxial testing at different confining pressures (L-20 Pc=20MPa, L-30 Pc=30MPa).

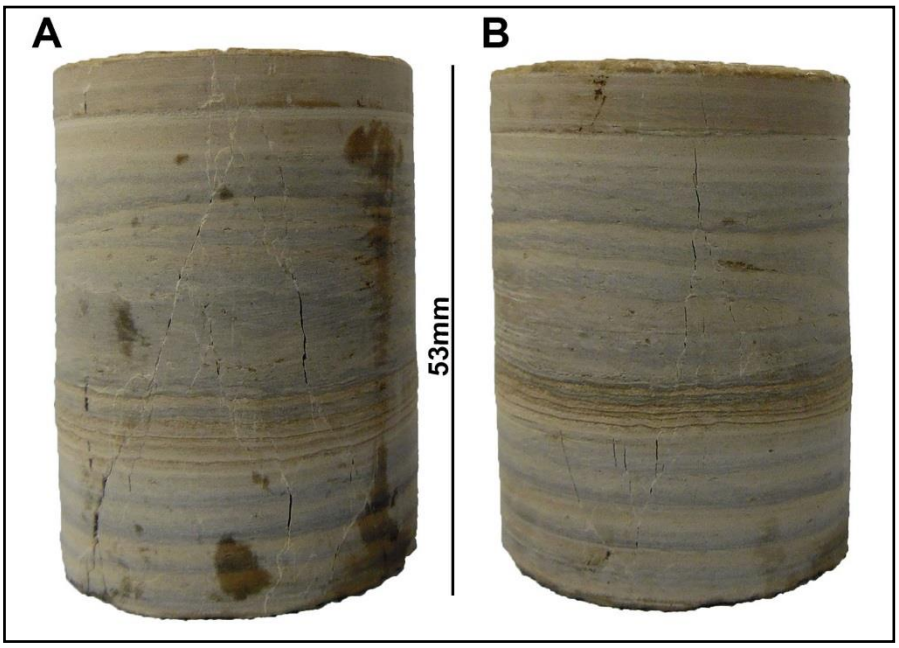

Figure 6. Laminite core plugs after triaxial deformation A: Laminite 20MPa confining pressure B: Laminite 30MPa confining pressure. Both samples show a combination of shear and now-open fractures on the plug surface.

3.2. 2D surface fracture analysis from XRT

The XRT edge scanline method allows for a quick quantitative analysis of fractures observed on the sample surface. It can be used instead of the classical but time consuming plotting of dip and strike values on a stereonet. Importantly it also has significant other advantages. It does not require that assumptions be made about what fracture trace combinations seen on the sample edge are part of the same fracture, also avoiding ambiguity over classification of branching fractures. It does not

 doi:10.20944/preprints201805.0171.v1

require the often difficult estimation of the fracture plane orientation from the surface traces. And it preserves fracture positional information.

I the edge scanline method the line of the fractures' intersections on the sample's cylindrical surface are the trace of the intersection between each fracture plane and the cylindrical surface, and as such will appear as a sinusoid when plotted on a flattened surface. They are referred to here as having a slope on an x-y plot of compass direction plotted on the x axis against vertical location on the y-axis (Figure 7). The fracture traces (Fig 7 B and D) follow the shapes observed on the sample photographs taken after testing (Figure 8) building confidence in the technique. A difference in fracture frequency in the samples could be linked to different mechanical characteristics such as the mechanical response of different assemblies of minerals, or lamination density or a combination of these but this relationship is outside the scope of this paper. Using 2D surface fracture reconstruction (Figure 7A and 7C) 20 fracture planes were identified from the plotted trends that could be easily traced and these are shown in Figures 7B and 7D. Using the surface fracture trace lines in Figures 7B and 7D the average dip angles were calculated for each reconstructed fracture plane and the values are shown in Table 2.

Preprints (www.preprints.org) | NOT PEER-REVIEWED | Posted: 10 May 2018 doi:10.20944/preprints201805.0171.v1

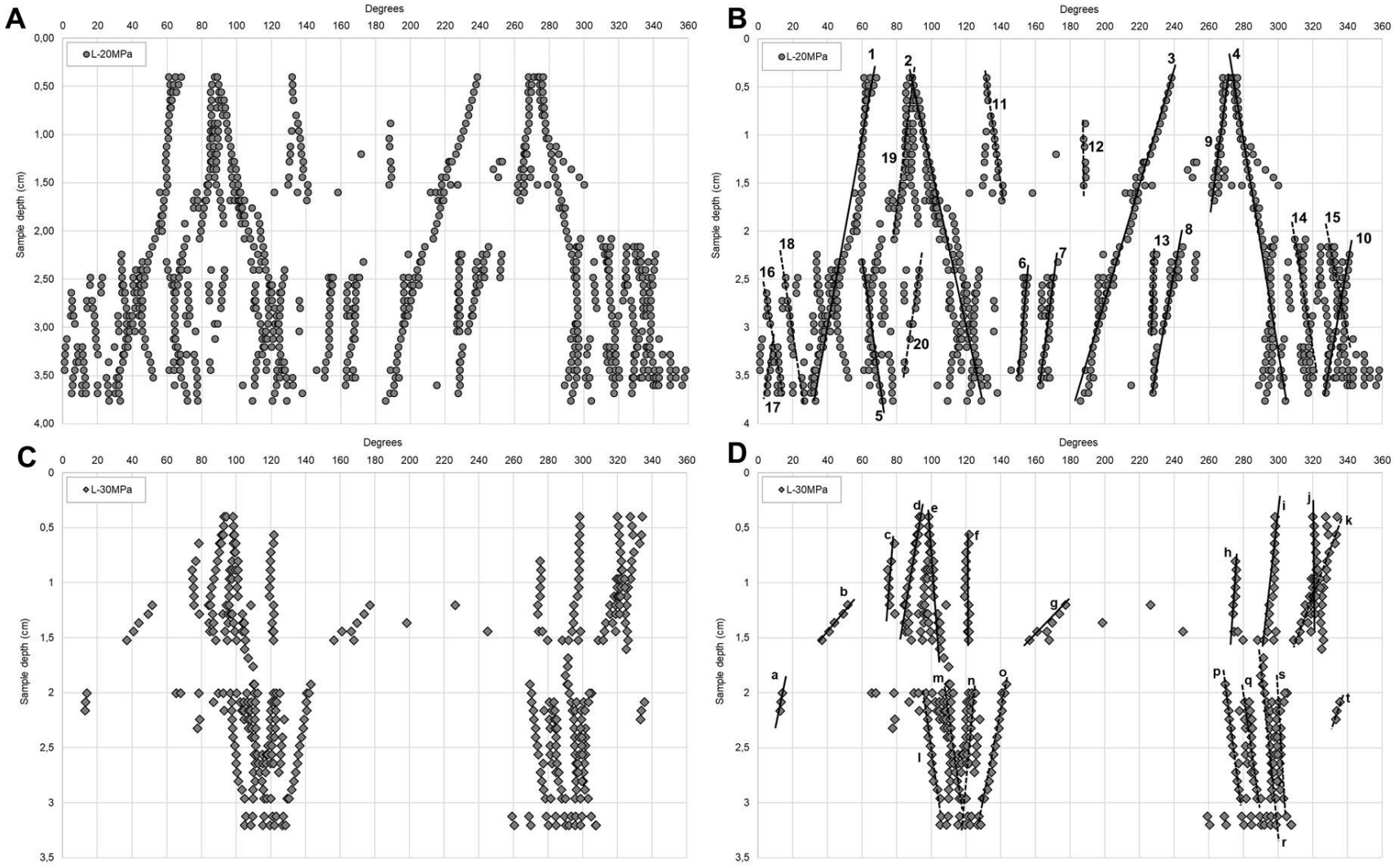

Figure 7. Surface fracture data for laminite core plugs deformed at 20MPa (A, B) and at 30MPa (C, D) confining pressure. A and C show the data generated by the new scanline method. B and D show the interpreted fractures to be used for subsequent average dip angle calculation. .

Preprints (www.preprints.org) | NOT PEER-REVIEWED | Posted: 10 May 2018 doi:10.20944/preprints201805.0171.v1

To validate this reconstruction approach to calculate reconstructed fracture plane dips approach the 2D reconstructed fracture planes (Figure 7) have been superimposed onto the core plug images (Figure 8).

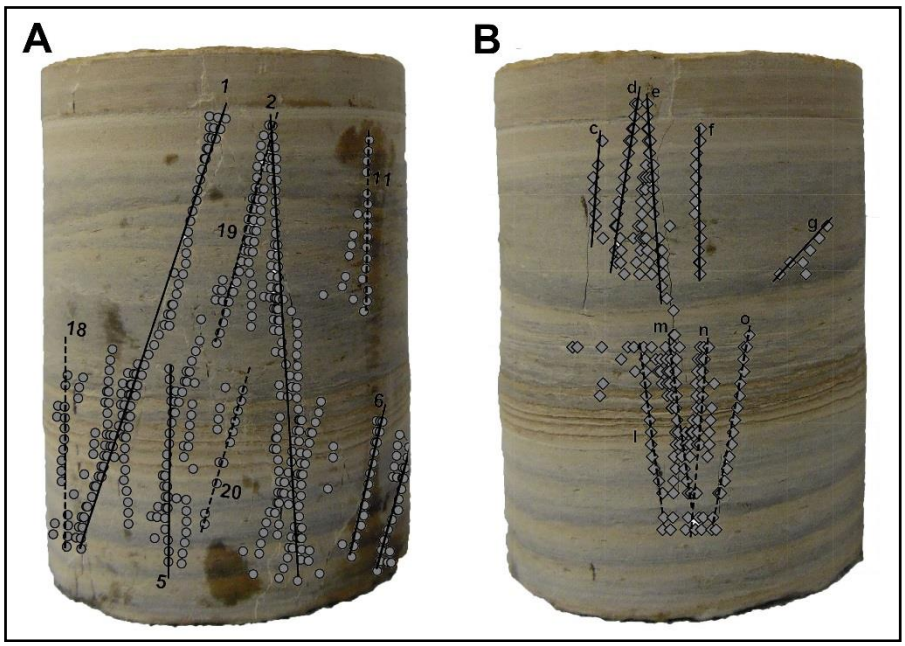

Figure 8. Surface fracture planes from the Edge scanline reconstruction superimposed onto the deformed core plug images

The reconstructed fracture faces line up well with the actual fractures in the core plugs. Any misalignments are due to the mismatch between a curved surface (core plug image) and the plane surface from the 2D reconstruction. However for comparison of fracture plane dips between different core plugs as well as with outcrop data we consider this a good match. To be able to compare reconstructed fracture plane dips the plotted degree values (Figure 7) have to be converted in to arc lengths using:

$$arc\ length\ (cm) = \frac{\Delta(x2-x1)angle}{360} \times 2\pi r \quad (1)$$

Where *x1* is the angle at the bottom of the fracture trace line, *x2* is the angle at the top of the fracture trace line and *r* is the radius of the sample. To calculate the arc length we assume that both angles are in the same plane to use the arc length in the calculation of the slope and therefore the overall dip equivalent angle of the fracture using:

$$dip\ equivalent\ angle\ (°) = arctan\left(\frac{y2-y1\ (cm)}{arc\ length\ (cm)}\right) \quad (2)$$

Where *y1* is the sample depth at the bottom of the fracture trace line and *y2* at the top. Reconstructed fracture plane dip values for negative slopes are corrected by subtracting the calculated value from 180° to allow for a geological nomination of fracture dip angles.

Table 2. Reconstructed fracture plane dip angles for laminite deformed at 20 and 30MPa confining pressure

Preprints (www.preprints.org) | NOT PEER-REVIEWED | Posted: 10 May 2018 doi:10.20944/preprints201805.0171.v1

L-20				L-30			
Fracture ID	dip equivalent (°)	Fracture ID	dip equivalent (°)	Fracture ID	dip equivalent (°)	Fracture ID	dip equivalent (°)
3	62.9	11	103.1	g	25.75	s	96.45
17	67.5	5	104.2	b	32.75	r	97.87
8	69.8	16	104.7	k	52.76	j	100.67
10	72.1	14	105.5	t	67.48	e	100.95
1	72.5	18	105.9	o	70.94	m	101.71
7	76.7	4	107.5	d	72.73	p	106.01
9	79.9	2	111.5	a	78.29	l	106.78
19	79.9	15	114.2	i	79.17	q	106.78
20	80.6			c	79.92		
6	80.9			n	84.08		
12	87.0			h	87.03		
13	87.6			f	88.02		

Even though this method allows for a quantitative presentation of the core plug surface fractures it does not allow for a detailed analysis of the fracture characteristics such as fracture connectivity or reconstruction of a 3D fracture network. Note here that a dip angle >90° indicates at 180° change in dip direction. There is a small difference in ranges of fracture slopes or dip equivalent angles between the two samples L-20 and L-30. L-30, deformed at the higher confining pressure, shows a higher range of fracture angles below a 90° dip with fractures dips as low as 25°. Whereas sample L-20 does not appear to have any surface fractures below 62° dip. This data allows for comparison of overall fracture angles and the identification of fracture sets and can be used for rose diagram analysis which can then be used for comparison with appropriate outcrop-derived data (Figure 8). The two samples were not scanned in the same compass orientation and direct comparison of the two fracture sets is not possible. However, at least for this limited dataset, it appears that a higher confining pressure concentrates fracture orientations into a smaller angular range, with one major and one minor fracture set being identified for the sample deformed at 30MPa (Fig 8B).

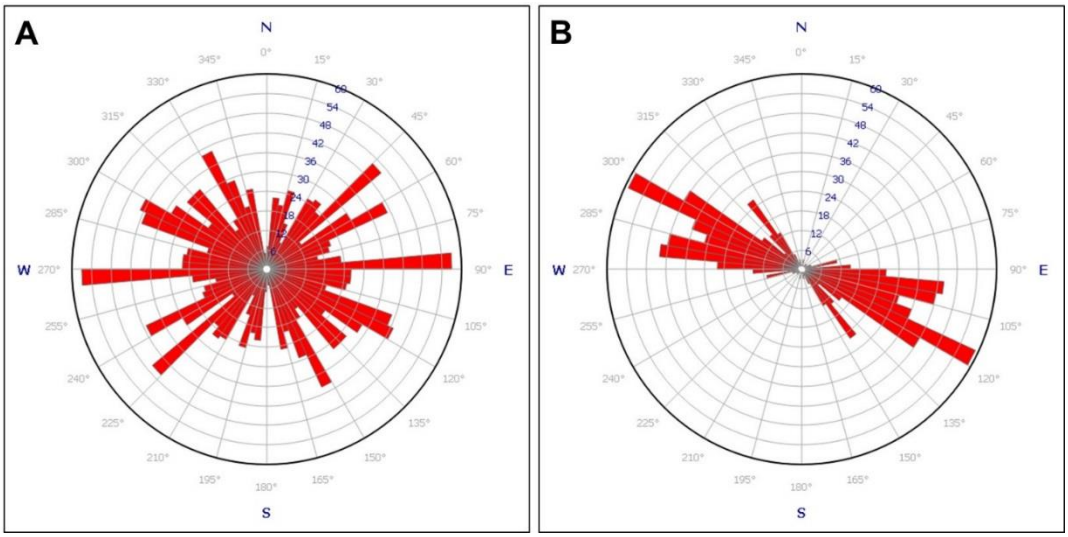

Figure 8. Rose diagram for laminites deformed at 20MPa (A) and 30MPa (B) confining pressure. Note that the scans were not taken in the same compass orientation and direct comparison is therefore not possible

Work from Miranda et al [29-31] shows that two fracture sets were identified in the laminite outcrop using data from scanlines parallel to lamination (Figure 9). Comparing this outcrop data

Preprints (www.preprints.org) | NOT PEER-REVIEWED | Posted: 10 May 2018 doi:10.20944/preprints201805.0171.v1

with the lab induced fracture sets shows that L-30 reproduces one of the patterns shown in the outcrop. The data from L-20 is too broad to identify distinct fracture sets. This could be due to the size of the sample plugs, to the axi-symmetric nature of the experimental loading, where the horizontal load, provided by confining pressure to the cylinder sides is constant, or due to the natural example reflecting more than one structural event. Despite this required data correction, the circular scanline can be considered a valid method of extracting lab-scale fracture data from core plug XRT images for comparison with outcrop and field data.

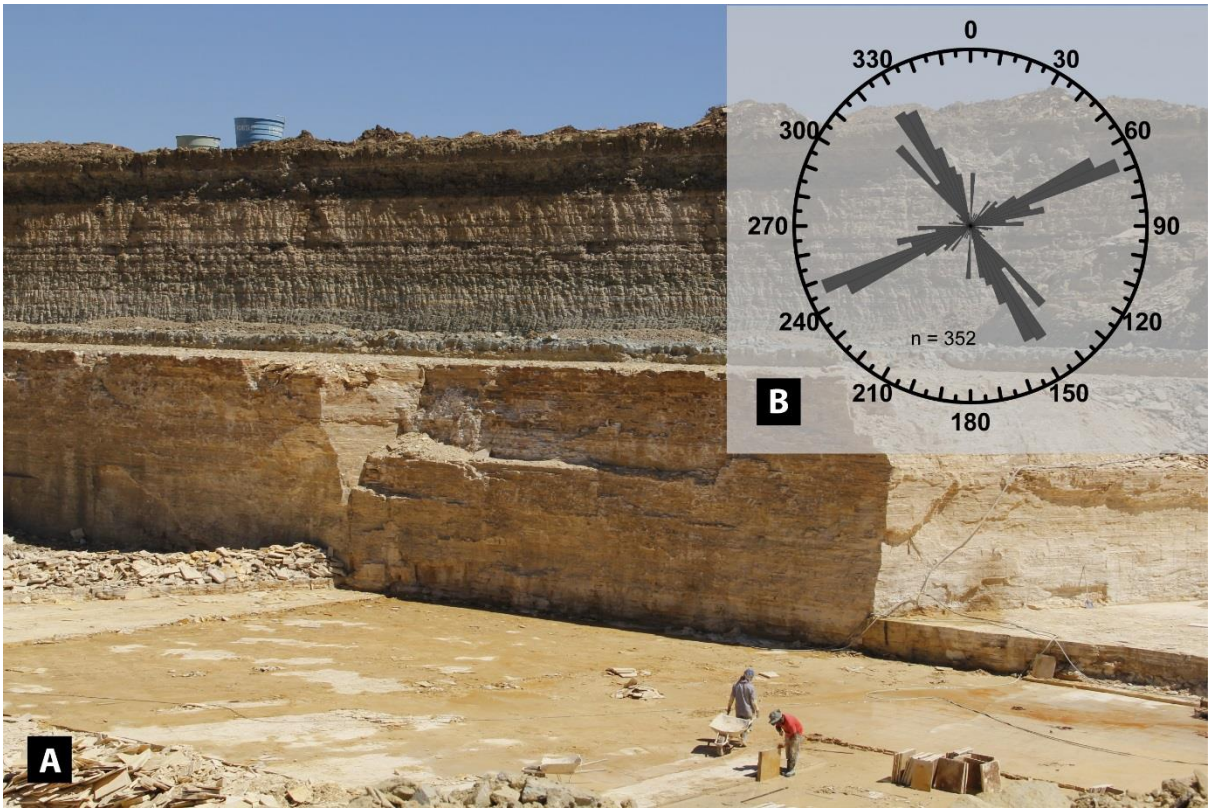

Figure 9. A: Laminite quarry (Tres Irmãos, near Santana do Cairi, Ceará State, NE Brazil) showing approximately horizontal and vertical quarry faces parallel and perpendicular to lamination B: Rose diagram of fractures from scanlines taken parallel to lamination plane.

3.3 Fracture aperture and distribution

Measurements from the XRT images at atmospheric conditions show that the fracture aperture distribution is larger for the sample deformed at 30MPa than for the sample deformed at 20MPa confining pressure. Sample L-30 also contains a larger number of fractures in the aperture range of 0.05mm to 0.1mm and exhibits fractures with >0.45mm aperture. But the fracture aperture range between >0.25mm and <0.45mm is missing in this sample. It is possible that the higher confining pressure leads to an accumulation of smaller fractures which then form bigger fractures. This is similar to strain localisation observed in granular materials that leads to the formation of shear bands [32]. Comparison with more laminate samples deformed at higher and lower confining pressures, including multiple samples at the same confining pressure is necessary to confirm or refute this trend.

Preprints (www.preprints.org) | NOT PEER-REVIEWED | Posted: 10 May 2018 doi:10.20944/preprints201805.0171.v1

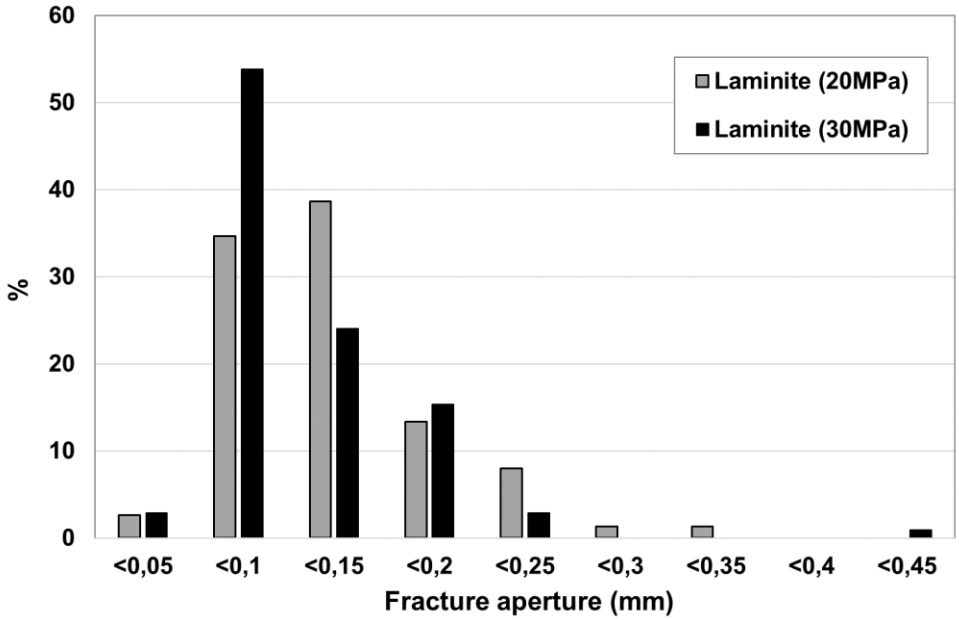

Figure 10. Fracture aperture distribution after deformation plotted against percentage of fractures in that category L-20 and L-30.

These fracture apertures fall within the range of apertures recorded from micro-scanlines using thin sections of samples from the quarry Tres Irmãos, near Santana do Cairi, Ceará State, NE Brazil (Figure 9), where a range of 0.01 to 0.2mm was recorded [30]. The values from the lab induced fractures also fall within the lower limit of fractures observed in the outcrop because fractures aperture is constrained by the samples size [29]. This shows that lab induced fractures combined with XRT image analysis can bridge the gap between thin section and outcrop scanlines.

One of the major issues in dealing with fracture datasets acquired from samples of very different sizes is the lack of ability to easily relate across different scales to allow for meaningful comparison of characteristics. This newly developed scanline method fills the gap between planar scanlines at the thin section scale and outcrop scale. It allows for comparison between naturally deformed laminites and experimentally deformed samples.

4. Conclusions

In this study we show that modifications of well-established scanlines methods can be on XRT images to provide quantitative data for comparison of fracture sets across scales, in particular it provides a link between thin section (micro-scanlines) and outcrop data. This allows for the validation of laboratory conditions for deformation experiments. We also show that fracture orientations can be used to compare between core plug samples and outcrop information if a consistent labelling convention for the laboratory samples is used for deformation and scanning.

Author Contributions: Stephanie G Zihms is the corresponding author for this article. They conceptualised the work for this article, with this they lead the investigation, data curation, formal analysis, methodology, project administration, validation, visualization, as well as writing the original draft of this article. Helen Lewis is the project PI and underwent the funding acquisition, they also supported the conceptualization, investigation, methodology and project administration for this research. They also supported the writing of this article by reviewing and editing the original draft. Tiago Miranda provided resources, mostly field data, research papers for field methods and supported the writing by reviewing the original draft article. Stephen Hall supported the investigation by conducting the x-ray tomography analysis and providing a written summary of the methodology for the original draft. James Somerville supported the investigation by conducting the triaxial deformationand supporting the formal analysis of the triaxial deformation data.

Funding: This research was funded by Royal Dutch Shell and Petrobras as part of the ICCR 2 research collaboration.

Acknowledgments: We would like to thank Petrobras and Shell for their sponsorship of the ICCR program and the permission to publish this work from the MechSeis2 project. In particular we would like to thank the MechSeis focal points for their help and support.

Conflicts of Interest: The authors declare no conflicts of interest. The funding sponsors had no role in the design of the study; in the collection, analyses, or interpretation of data; in the writing of the manuscript, and in the decision to publish the results.

References

1. Dimmen, V., et al., Quantifying structural controls on fluid flow: Insights from carbonate hosted fault damage zones on the Maltese Islands. Jounrnal of Structural Geology, 2017. 101: p. 43-57.
2. Panza, E., et al., Fracture stratigraphy and fluid flow properties of shallow-water, tight carbonates: The case study of the Murge Plateau (southern Italy). Marine and Petroleum Geology, 2016. 73: p. 350-370.
3. Guerriero, V., et al., A permeability model for naturally fractured carbonate reservoirs. Marine and Petroleum Geology, 2013. 40: p. 115-134.
4. Couples, G.D., Geomechanical impacts on flow in fractured reservoirs. Geological Society, London, Special Publications, 2013. 374(1): p. 145-172.
5. Jia, L., M. Chen, and Y. Jin, 3D imaging of fractures in carbonate rocks using X-ray computed tomography technology. Carbonates and Evaporites, 2013. 29(2): p. 147-153.
6. Arzilli, F., et al., Using synchrotron X-ray microtomography to characterize the pore network of reservoir rocks: A case study on carbonates. Advances in Water Resources, 2015.
7. Christe, P., et al., An X-ray computed tomography-based index to characterize the quality of cataclastic carbonate rock samples. Engineering Geology, 2011. 117(3-4): p. 180-188.
8. De Kock, T., et al., A pore-scale study of fracture dynamics in rock using X-ray micro-CT under ambient freeze-thaw cycling. Environ Sci Technol, 2015. 49(5): p. 2867-74.
9. Ji, Y., et al., Characterization of pore structure and strain localization in Majella limestone by X-ray computed tomography and digital image correlation. Geophysical Journal International, 2015. 200(2): p. 699-717.
10. Kodama, J., et al., Observation of Fracture Process of Rocks Subjected to Freeze-Thaw Cycles Using X-ray CT, in 8th Asian Rock Mechanics Symposium, Shimuzi, Kaneko, and Kodama, Editors. 2014: Sapporo, Japan.
11. Krakowska, P., et al., Computed X-ray microtomography as the useful tool in petrophysics: A case study of tight carbonates Modryn formation from Poland. Journal of Natural Gas Science and Engineering, 2016. 31: p. 67-75.
12. Teles, A.P., et al., Analysis of subterranean Pre-salt carbonate reservoir by X-ray computed microtomography. Journal of Petroleum Science and Engineering, 2016. 144: p. 113-120.
13. Cnudde, V. and M.N. Boone, High-resolution X-ray computed tomography in geosciences: A review of the current technology and applications. Earth-Science Reviews, 2013. 123: p. 1-17.
14. Saenger, E.H., et al., Digital carbonate rock physics. Solid Earth, 2016. 7(4): p. 1185-1197.
15. Wang, F., et al., Petrophysical properties analysis of a carbonate reservoir with natural fractures and vugs using X-ray computed tomography. Journal of Natural Gas Science and Engineering, 2016. 28: p. 215-225.

16. Deng, H., J.P. Fitts, and C.A. Peters, Quantifying fracture geometry with X-ray tomography: Technique of Iterative Local Thresholding (TILT) for 3D image segmentation. Computational Geosciences, 2016. 20(1): p. 231-244.

17. Baud, P., A. Schubnel, and T.-f. Wong, Dilatancy, compaction, and failure mode in Solnhofen limestone. Journal of Geophysical Research, 2000. 105(B8): p. 19289.

18. Brantut, N., et al., Mechanisms of time-dependent deformation in porous limestone. Journal of Geophysical Research: Solid Earth, 2014. 119(7): p. 5444-5463.

19. Vajdova, V., et al., Micromechanics of inelastic compaction in two allochemical limestones. Journal of Structural Geology, 2012. 43: p. 100-117.

20. Lecomte, E., C. Chalak, and H. Lewis. Evaluation of a fault zone in a carbonate hydrocarbon reservoir. in 23rd ALERT Workshop: Geomechanics for Energy Production. 2012. Aussois, France.

21. Calvo, J.P., et al., Microdeformation of lacustrine laminite sequences from Late Miocene formations of SE Spain: an interpretation of loop bedding. Sedimentology, 1998. 45: p. 279-292.

22. Mauldon, M., Estimating Mean Fracture Trace Length and Density from Observations in Convex Windows. Rock Mechanics and Rock Engineering, 1998. 31(4): p. 201-216.

23. Mauldon, M., W.M. Dunne, and M.B. Rohrbaugh Jr, Circular scanlines and circular windows: new tools for characterizing the geometry of fracture traces. Journal of Structural Geology, 2001. 23(2–3): p. 247-258.

24. Schindelin, J., et al., Fiji: an open-source platform for biological-image analysis. Nat Meth, 2012. 9(7): p. 676-682.

25. Ortega, O.J., R.A. Marrett, and S.E. Laubach, A scale-independent approach to fracture intensity and average spacing measurement. AAPG Bulletin, 2006. 90(2): p. 193-208.

26. Ma, J., et al., A Multi-Scale Framework for Digital Core Analysis of Gas Shale at Millimeter Scales, in Proceedings of the 2nd Unconventional Resources Technology Conference. 2014.

27. Buckman, J., et al., Quantifying Porosity through Automated Image Collection and Batch Image Processing: Case Study of Three Carbonates and an Aragonite Cemented Sandstone. Geosciences, 2017. 7(3).

28. Kling, T., et al., Simulating stress-dependent fluid flow in a fractured core sample using real-time X-ray CT data. Solid Earth, 2016. 7(4): p. 1109-1124.

29. Miranda, T., et al., Natural fracture characterization in Aptian carbonates, Araripe Basin, NE Brazil, in 76th EAGE Conference & Exhibition. 2014: Amsterdam, The Netherlands.

30. Miranda, T., et al., Aplicação da técnica de scanline à modelagem geológica/geomecânica de sistemas de fraturamento nos depósitos carbonáticos e evaporíticos da Bacia do Araripe, NE do Brasil. Boletim de Geociências da Petrobras, 2011. 20(1/2): p. 305-326.

31. Miranda, T., et al., Petrophysics and petrography of Aptian tight carbonate reservoir, Araripe Basin, NE Brazil, in 78th EAGE Conference & Exhibition. 2016: Vienna, Austria.

32. Desrues, J., P. Besuelle, and H. Lewis, Strain localization in geomaterials. Geological Society, London, Special Publications, 2007. 289(1): p. 47-73.